MNRAS **451,** 3615–3626 (2015) doi:10.1093/mnras/stv1221

An extended star formation history in an ultra-compact dwarf

Mark A. Norris,[1⋆] Carlos G. Escudero,[2,3,4] Favio R. Faifer,[2,3,4] Sheila J. Kannappan,[5] Juan Carlos Forte[4,6] and Remco C. E. van den Bosch[1]

[1]*Max Planck Institut für Astronomie, Königstuhl 17, D-69117 Heidelberg, Germany*
[2]*Facultad de Cs. Astronómicas y Geofísicas, UNLP, Paseo del Bosque S/N, 1900 La Plata, Argentina*
[3]*Instituto de Astrofísica de La Plata (CCT La Plata – CONICET – UNLP), Paseo del Bosque S/N, 1900 La Plata, Argentina*
[4]*Consejo Nacional de Investigaciones Científicas y Técnicas, Rivadavia 1917, C1033AAJ Ciudad Autónoma de Buenos Aires, Argentina*
[5]*Department of Physics and Astronomy UNC-Chapel Hill, CB 3255, Phillips Hall, Chapel Hill, NC 27599-3255, USA*
[6]*Planetario Galileo Galilei, Secretaría de Cultura, Ciudad Autónoma de Buenos Aires, Argentina*

Accepted 2015 May 29. Received 2015 May 28; in original form 2015 April 2

ABSTRACT

There has been significant controversy over the mechanisms responsible for forming compact stellar systems like ultra-compact dwarfs (UCDs), with suggestions that UCDs are simply the high-mass extension of the globular cluster population, or alternatively, the liberated nuclei of galaxies tidally stripped by larger companions. Definitive examples of UCDs formed by either route have been difficult to find, with only a handful of persuasive examples of stripped-nucleus-type UCDs being known. In this paper, we present very deep Gemini/GMOS spectroscopic observations of the suspected stripped-nucleus UCD NGC 4546-UCD1 taken in good seeing conditions (<0.7 arcsec). With these data we examine the spatially resolved kinematics and star formation history of this unusual object. We find no evidence of a rise in the central velocity dispersion of the UCD, suggesting that this UCD lacks a massive central black hole like those found in some other compact stellar systems, a conclusion confirmed by detailed dynamical modelling. Finally, we are able to use our extremely high signal-to-noise spectrum to detect a temporally extended star formation history for this UCD. We find that the UCD was forming stars since the earliest epochs until at least 1–2 Gyr ago. Taken together these observations confirm that NGC 4546-UCD1 is the remnant nucleus of a nucleated dwarf galaxy that was tidally destroyed by NGC 4546 within the last 1–2 Gyr.

Key words: galaxies: dwarf – galaxies: evolution – galaxies: formation – galaxies: kinematics and dynamics – galaxies: stellar content.

1 INTRODUCTION

Since their discovery a decade and a half ago (Hilker et al. 1999; Drinkwater et al. 2000), ultra-compact dwarfs (UCDs; Phillipps et al. 2001) have proven to be highly enigmatic and controversial. Their structural parameters (size, mass, and central velocity dispersion) place them uneasily between star clusters, such as classical globular clusters (GCs), and bona fide galaxies. Their transitional location in scaling relations led to their exact origin being strongly debated, between those who favoured their formation as the most massive star clusters (see e.g. Fellhauer & Kroupa 2002, 2005; Brüns & Kroupa 2012; Mieske, Hilker & Misgeld 2012) and those that considered them the remnant nuclei of galaxies that have been tidally stripped (see e.g. Bekki & Couch 2003; Drinkwater et al. 2003; Pfeffer & Baumgardt 2013).

However, in recent years a consensus has begun to emerge that as a group UCDs are a 'mixed bag', made up of both massive GCs and stripped galaxy nuclei (Hilker 2006; Brodie et al. 2011; Chiboucas et al. 2011; Da Rocha et al. 2011; Norris & Kannappan 2011; Forbes et al. 2014; Norris et al. 2014a; Pfeffer et al. 2014). This view has developed because of the dual realization that while most UCDs have properties consistent with those expected of GCs (including age, metallicity, alpha-element enhancement) and appear in numbers consistent with their being the bright end of the GC luminosity function (see e.g. Hilker 2006; Norris & Kannappan 2011; Mieske et al. 2012), some UCDs are undeniable outliers, and have properties more consistent with a galactic origin (see below). Additional evidence for a stripped-nucleus UCD population comes from theoretical simulations which indicate that stripping should be an effective method of creating UCD-like objects (Bekki & Couch 2003; Pfeffer & Baumgardt 2013), and should be relatively common in a Λ cold dark matter cosmology (e.g. Pfeffer et al. 2014), where minor merger events are common, particularly at early epochs.

⋆ E-mail: norris@mpia.de

Unfortunately, despite this emerging consensus, very few UCDs are easily and definitively classifiable into either of the two groups, making it difficult to estimate the efficiency of stripped UCD formation with any accuracy. In part, this is because of significant overlaps in the predicted properties of either type of object. But additionally, it is also due to the fact that those definitive signatures of UCD origin are observationally difficult to detect. For example, one of the clearest discriminants between massive GCs and stripped nuclei is to be found in the presence or absence of a central massive black hole. Many galaxies are observed to harbour a supermassive black hole (SMBH), with the occupation fraction increasing with galaxy mass until essentially all galaxies more massive than $M_\star \sim 10^{10.5}$ M$_\odot$ (e.g. Decarli et al. 2007; Miller et al. 2015) are thought to host SMBHs. After tidal stripping of their host galaxies, these SMBHs should remain within the central bound star clusters, now transformed into a UCD. However, while the presence of an SMBH is definitive proof that a particular UCD formed in a tidal stripping event, the converse is not true, as many lower mass galaxies are not found to have SMBHs (e.g. M33 and NGC 205; Gebhardt et al. 2001; Valluri et al. 2005). Regardless, to detect the signature of a black hole, even a relatively massive one, in a faint object with a size on the sky of <1 arcsec requires very large telescopes combined with either excellent natural seeing or adaptive optics (AO) observations.

To date only two high spatial resolution spectroscopic observations of UCDs are in the literature. Making use of good natural seeing conditions, Frank et al. (2011) used IFU observations to study Fornax UCD3, finding weak rotation ($\sim$3 km s^{-1}) but no clear sign of either the presence of a large black hole or of dark matter (another clear signature of a galactic origin). In contrast, Seth et al. (2014) examined the unusually dense UCD M60-UCD1 (Strader et al. 2013) finding that it contained a black hole comprising 15 per cent of its total mass. In this case, high-resolution AO-assisted spectroscopy was key; the dynamical-to-stellar mass ratio of this UCD as measured in natural seeing data is not unusual (Strader et al. 2013; Forbes et al. 2014). In fact, even when including the influence of the black hole, Seth et al. (2014) find that the mass-to-light ratio (M/L) of M60-UCD1 is still consistent with that of massive GCs (although the stellar M/L decreases by 40 per cent compared to the no black hole model). This observation strongly hints that many more massive black holes in UCDs remain to be discovered. Many other massive UCDs do indeed display unusual dynamical mass-to-stellar mass ratios indicative of the likely presence of a large black hole (e.g. S999 with $M_{\rm dyn}/{\rm M}_\odot = 8.2$; Janz et al. 2015), but without higher spatial resolution data no definitive conclusions can be drawn.

One other conclusive proof of a galactic origin that until now has not been examined is whether or not a UCD had an extended star formation history (SFH). This approach has the benefit that while good signal-to-noise (S/N) spectroscopy is required, very high spatial resolution (and consequently AO-assisted) observations are not. Despite recent discoveries of multiple stellar populations within Milky Way GCs (see e.g. Gratton, Carretta & Bragaglia 2012), GCs are still a very good approximation of idealized single stellar populations. UCDs which formed as giant GCs should be similar, or if they formed from the merger of several normal GCs in a dense star-forming region, the age spread should at least be small ($\lesssim$200 Myr; Fellhauer & Kroupa 2005). The same is not true of nuclear star clusters (NSCs), some of which are observed to have recent or ongoing star formation (Rossa et al. 2006; Seth et al. 2006; Walcher et al. 2006; Georgiev & Böker 2014), indicating very extended formation times. Therefore, detecting an extended SFH would be a true 'smoking gun' of a stripped-nucleus origin for a UCD.

In this paper, we examine the UCD of NGC 4546 for signs that it is of galactic origin. NGC 4546 is a potentially fruitful place to look for a stripped-nucleus UCD, because it is located in a lower density environment (i.e. not a cluster core), where it is possible for gas-rich (and hence young) galaxies to undergo low-speed interactions of the type necessary to lead to tidal stripping. In galaxy clusters only old populations exist, making it difficult to separate stripped-nucleus UCDs from the equally old GC population, while in the field it is possible to form stripped-nucleus UCDs that are younger than the GC population of the associated galaxy. In Norris & Kannappan (2011), we have already shown that there are several good reasons to believe that NGC 4546-UCD1 is a former nucleus. First, this UCD is $\sim$3 mag brighter than the brightest GCs of NGC 4546, far too bright to be simply explained as the bright end of the GC luminosity function. Secondly, it is observed to counter-rotate its host galaxy, and in the same sense as a counter-rotating gas feature seen in the host galaxy. Thirdly, its alpha-element enhancement ratio [α/Fe] is close to solar, indicating that the gas that formed it was enriched over an extended period, while most GCs are [α/Fe] enhanced indicating very rapid star formation. Finally, it is young, around 3 Gyr, while its host galaxy is uniformly old (>10 Gyr). It is these facts, combined with its relative brightness ($V = 17.6$) and its relative closeness, only $\sim$13 Mpc ($M - m = 30.58 \pm 0.2$) away, that make this object a prime candidate to search for signatures of a galactic origin for a UCD.

2 OBSERVATIONS

2.1 Gemini/GMOS spectroscopy

The Gemini/GMOS (Hook et al. 2004) spectroscopy utilized in this paper was observed in the period 2013 July 2 to 2014 January 7 as part of Gemini programme GS-2013A-Q-26. The main purpose of this programme is to probe the connection, if any, between NGC 4546-UCD1 and the GC system of NGC 4546. The results of this larger study will be presented in two forthcoming papers focusing on the photometric (Faifer et al., in preparation) and spectroscopic properties (Escudero et al., in preparation) of the UCD and GC system. In this paper, we focus on the information provided by the spectrum of NGC 4546-UCD1.

The spectroscopy described here comprises 12 usable exposures, each of exposure time 1850 s, observed with the B1200 grating with the UCD being observed through a 0.5 arcsec MOS slitlet. Four additional exposures were obtained but not used in this analysis because the instrument was significantly out of focus and the spectral resolution was a factor of $\sim$2 worse than desired. The resolution of the 12 good individual exposures varied from 1.26 to 1.57 Å FWHM (full width at half-maximum) as measured using isolated lines on the calibration arc spectra and the 5197 Å sky line which was visible on 11 of 12 of our science exposures. The spectral resolution measured from the same sky line on the summed 2D science frame was 1.41 $\pm$ 0.06 Å with the line being well fitted by a Gaussian line spread function. The spectral setup utilized was sampled with 0.5 Å pixels over a wavelength range of 4080–5575 Å. The seeing of the individual exposures varied from 0.5 to 0.9 arcsec with the median value being $\sim$0.7 arcsec as measured from the spatial distribution of the summed 2D spectrum of a confirmed Milky Way star (i.e. a point source). The alignment accuracy of the slitlets as measured from the alignment images was around 0.1 arcsec, for all but one exposure which was offset by around 0.2 arcsec.

The reduction of the GMOS spectroscopy was initially similar to that outlined in Norris et al. (2008). The Gemini IRAF package was used to carry out overscan subtraction, bias subtraction, flat-fielding, extraction of the individual 2D slitlets, wavelength calibration, and rectification. Further reduction was then achieved using a set of custom IDL scripts. These scripts spatially rectified the 2D spectrum by tracing the peak of the light distribution, corrected for heliocentric motion (extremely important as the heliocentric velocity varies from -30 to $+29\,\mathrm{km\,s^{-1}}$ for this data set), sky subtracted the individual exposures, and finally spatially aligned and co-added the individual exposures (with a clipping to reject the unexposed chip gaps and bad pixels). Finally, IRAF APALL was used to trace and extract a single integrated spectrum of the UCD, while an IDL script was used to extract a series of spectra spatially binned across the slit, each of which had a minimum S/N of 35 $\mathrm{\AA^{-1}}$.

Because of the relative brightness of the UCD compared to the GC targets on the same mask (the UCD is $\sim$3 mag brighter), the S/N of the resulting integrated spectrum is excellent. The integrated spectrum has an S/N of between 50 $\mathrm{\AA^{-1}}$ at 4100 Å and 200 $\mathrm{\AA^{-1}}$ at 5500 Å.

Flux calibration was achieved using an exposure of EG131 obtained as part of this science programme using the same observational setup as the main science data, except that the standard star was observed through a 0.5-arcsec-wide longslit, rather than the MOS mask. The reduction of the standard star data followed the same procedure as the science data.

2.2 Gemini/GMOS imaging

As well as spectroscopic observations we have also obtained deep imaging of the environs of NGC 4546, primarily in order to select GCs for spectroscopic follow-up. However, this deep photometry is also extremely useful in estimating the stellar mass of NGC 4546-UCD1. The imaging was obtained with GMOS and comprises 4×100 s exposures in the g', r', i' filters and 4×290 s exposures in the z' filter (Fukugita et al. 1996). GMOS imaging provides a field of view of 5.5 arcmin $\times$ 5.5 arcmin, and we used 2×2 binning, giving a pixel scale of 0.146 arcsec pixel^{-1}. The subexposures were dithered to remove the gaps between the three GMOS CCDs and also to facilitate cosmic ray removal.

The raw data were processed with the Gemini-GMOS IRAF package (e.g. gprepare, gbias, giflat, gireduce, and gmosaic), using appropriate bias and flat-field frames from the Gemini Science Archive (GSA). As final step in the reduction process, the resulting images for each filter were aligned and co-added using the task IMCOADD.

To perform the photometry of the UCD, we first modelled and subtracted the sky background and light from the halo of NGC 4546. To do this, we used an iterative combination of the SExtractor software (Bertin & Arnouts 1996) and median filtering within IRAF (see e.g. Faifer et al. 2011). This procedure provides a galaxy light-subtracted image. Aperture photometry was then obtained for NGC 4546-UCD1, using the PHOT task with a fixed 4.3 arcsec ($>10R_e$ for this UCD) aperture. The derived magnitudes are entirely consistent with ones derived using an alternative curve-of-growth analysis. Standard star fields, downloaded from the GSA, were used to achieve the transformation to the standard system. Finally, we applied the galactic extinction coefficients given by Schlafly & Finkbeiner (2011) ($A_g = 0.112, A_r = 0.077, A_i = 0.057, A_z = 0.043$). Table 1 gives the photometry for NGC 4546-UCD1.

Table 1. Properties for NGC 4546-UCD1.

Property	Value
RA (J2000)	12:35:28.7
Dec. (J2000)	–03:47:21.1
Distance	13.06 ± 1.26 Mpc
Photometry	
B	18.57 ± 0.05 mag[a]
V	17.64 ± 0.04 mag[a]
R	17.04 ± 0.03 mag[a]
g'	18.13 ± 0.01 mag
r'	17.39 ± 0.01 mag
i'	17.01 ± 0.01 mag
z'	16.73 ± 0.05 mag
J	15.70 ± 0.11 mag[a]
H	14.69 ± 0.23 mag[a]
K_s	14.86 ± 0.17 mag[a]
3.6 μm	14.40 ± 0.16 mag
Derived quantities	
R_e	25.54 ± 1.30 pc
V	$1225.6 \pm 0.3\,\mathrm{km\,s^{-1}}$
σ	$23.5 \pm 2.5\,\mathrm{km\,s^{-1}}$
σ_∞	$21.6 \pm 2.5\,\mathrm{km\,s^{-1}}$
$M_{\star,\mathrm{SED}}$	$3.27^{+0.85}_{-0.90} \times 10^7\,\mathrm{M_\odot}$
$M_{\star,3.6\,\mu\mathrm{m}}$	$3.11^{+0.66}_{-0.66} \times 10^7\,\mathrm{M_\odot}$
M_{vir}	$2.17^{+0.51}_{-0.51} \times 10^7\,\mathrm{M_\odot}$
M_{dyn}	$2.59^{+0.49}_{-0.49} \times 10^7\,\mathrm{M_\odot}$
Luminosity-weighted stellar populations	
Age	3.0 ± 0.05 Gyr
[Z/H]	0.29 ± 0.01 dex
[α/Fe]	-0.02 ± 0.02 dex

Notes. [a]The B, V, R, J, H, & K_s photometry is from Norris & Kannappan (2011).

2.3 *Spitzer* IRAC imaging

Several papers have recently demonstrated that the *WISE* W1 or *Spitzer* IRAC 1 bands at 3.4/3.6 μm are an almost ideal stellar mass tracer for older (age >2 Gyr) stellar populations (see e.g. Meidt et al. 2014; Norris et al. 2014b; Querejeta et al. 2014), and even for actively star-forming discs (McGaugh & Schombert 2015). Furthermore, as shown in Norris et al. (in preparation), these photometric bands are remarkably insensitive to the detailed SFH of a stellar population, especially when combined with a spectroscopically derived luminosity-weighted age and metallicity for the stellar population. In such cases, the systematic uncertainty on an M/L introduced by imperfect knowledge of the SFH is always less than 15 per cent, when the luminosity-weighted age is >2 Gyr, although systematic uncertainties due to stellar population synthesis modelling and assumed initial mass function (IMF) can be considerably higher. Given these advantages, we have examined archival *Spitzer Space Telescope* IRAC 1 (3.6 μm) band imaging of NGC 4546 in order to derive a stellar mass for NGC 4546-UCD1 that can be compared to estimates made using more common approaches [i.e. Spectral Energy Distribution (SED) fitting].

The observations that we utilize were observed in 2008 July as part of programme 50630 (PI: van der Wolk), investigating the interstellar medium, star formation, and nuclei of the SAURON sample of early-type galaxies. The exposure time was 30 s, and in

our analysis we make use of the IRAC 1 map produced by the Spitzer Heritage Archive.[1]

The first step in our analysis is to subtract the bright halo of NGC 4546 which would compromise photometry of the UCD. To do that, we make use of a multistep approach. First, we run SExtractor (Bertin & Arnouts 1996) in a very sensitive mode, with detection threshold of 1.5σ, and a very small background mesh value (16 pixels), in order to detect all sources, even those buried deep in the galaxy halo. The output of this analysis is an output image segmented into detected sources; this image is then converted into a pixel mask image, where every source is masked, other than NGC 4546 itself. We then use the IRAF task ELLIPSE in combination with the pixel mask to fit NGC 4546, with the resulting best-fitting model being subtracted from the original input to produce a galaxy-subtracted image.

Because the compact UCD (with $R_e = 0.4$ arcsec) is unresolved in IRAC 1 imaging (resolution $\sim$1.7 arcsec), we use aperture photometry to measure its integrated magnitude. Following the procedure outlined in Reach et al. (2005), we use a 10 pixel aperture (1 pixel = 0.6 arcsec) and a sky annulus of 12–20 pixels. Using the conversions provided in Reach et al. (2005) from MJy to magnitudes, we derive a total integrated magnitude in the IRAC 1 band of 14.40 ± 0.16 mag (where we have added a conservative error of 0.15 mag in quadrature to the photometric error, to account for the poorly constrained error due to the galaxy background and IRAC scattered light) for the UCD.

2.4 Additional data

In addition to the new data described above, our analysis also makes use of SOAR/Goodman optical imaging in the *B*, *V*, and *R* bands, and 2MASS *J*, *H*, and K_s imaging. The reduction and analysis of both sets of data was described in Norris & Kannappan (2011). We also utilize the only available *Hubble Space Telescope* (*HST*) imaging of NGC 4546, a single Wide Field Planetary Camera 2 (WFPC2) image in the *F*606*W* filter, the analysis of which was also described in Norris & Kannappan (2011).

3 RESULTS

3.1 Kinematics

We use the penalized pixel fitting code PPXF (Cappellari & Emsellem 2004) to measure the UCD kinematics. As in Norris et al. (2014a), we make use of the stellar population synthesis models of Maraston & Strömbäck (2011) as the template spectra. In particular, we use the high-resolution (0.55 Å FWHM) ELODIE-based Single Stellar Population (SSP) models, because they are currently the only comprehensive set of SSP models (as opposed to libraries of individual stellar spectra) available with resolution higher than our spectra (1.41 Å).

3.1.1 Integrated kinematics

We first examine the kinematics of the integrated spectrum of NGC 4546-UCD1. We fit the integrated spectrum over the wavelength range 4120–5530 Å, masking two regions affected by residuals from chip gaps (around 4600 and 5080 Å). We first attempted fitting the first four moments of the line-of-sight velocity distribution (LOSVD); however, the higher order moments h_3 and h_4 were consistent with zero and so we refit using only the first two moments, the velocity and velocity dispersion. We estimate the uncertainties on the measured parameters using 100 Monte Carlo resimulations of the data with the measured uncertainties on the spectra and the spectral resolution. Fig. 1 shows the result of the fitting procedure. It is clear that the fit is excellent, with only slight mismatch between the template and the model in the region where problems due to the chip gaps remain. The excellent fit also indicates that as expected there is no significant Hβ or [O III] emission present in the UCD.

The measured recessional velocity is in good agreement with that measured from the previously presented lower resolution SOAR/Goodman spectroscopy (Norris & Kannappan 2011), and also with the remeasured velocity derived from the higher resolution SOAR/Goodman spectrum presented in Norris et al. (2014a) after this spectrum was reanalysed using the same method as here.[2] It is interesting that the measurement of velocity dispersion determined in Norris et al. (2014a) (21.8 ± 2.5) and the one determined here (23.5 ± 2.5) agree so well, despite the significantly improved seeing available in the observations with GMOS ($\sim$0.7 arcsec versus $\sim$1.4 arcsec). This is suggestive that the velocity dispersion of NGC 4546-UCD1 is not strongly centrally peaked.

3.1.2 Spatially resolved kinematics

We next turn to our attempt to extract spatially resolved kinematics from our spectroscopy. As described previously, we spatially binned our spectrum along the slit to a minimum S/N of 35 Å^{-1} (as measured in the region 5000–5050 Å); this yielded 11 separate spectra across the UCD, with the central 9 pixels all reaching that S/N with a single spatial pixel. We then fit each spectrum using exactly the same procedure outline above.

Fig. 2 shows the result of the fitting procedure. We are able to detect rotation of amplitude 1.3 km s^{-1} (as measured using a probabilistic min/max procedure to determine the most likely lower and upper rotation velocity) across the UCD, with a central recessional velocity that is very consistent with that derived from the integrated spectrum.

The small amplitude of rotation is close to the limit that our spectroscopic setup would be expected to reliably recover; we have therefore examined how robust this detection is to changes in spatial binning, wavelength range fit, and number of LOSVD moment fit. In part, we do this to attempt to probe the effect of systematic uncertainties such as template mismatch, etc. We find that while the exact amplitude of the rotation varies between 1 and 2 km s^{-1}, the detection of rotation and its sign (i.e. which side recedes or approaches) are a robust result of the fitting procedure.

The general shape of the rotation curve is also intriguing, as the apparent reversal in direction around -0.5 arcsec is also a robust result of the kinematic fitting procedure. The shape itself could be indicative of disturbed kinematics, such as a counter-rotating stellar component. These features, known as kinematically decoupled cores, have been observed in a range of galaxy types from massive early types (e.g. Emsellem et al. 2007) to low-mass dwarf ellipticals where they typically display both counter-rotation and younger stellar populations (Toloba et al. 2014). In addition, complex counter-rotating structures have been uncovered in several NSCs (Seth et al.

[1] http://sha.ipac.caltech.edu/applications/Spitzer/SHA

[2] The previous estimation used IRAF's FXCOR to derive the velocity, and included an incorrect sign for the heliocentric correction for this object leading to an apparent offset in velocity.

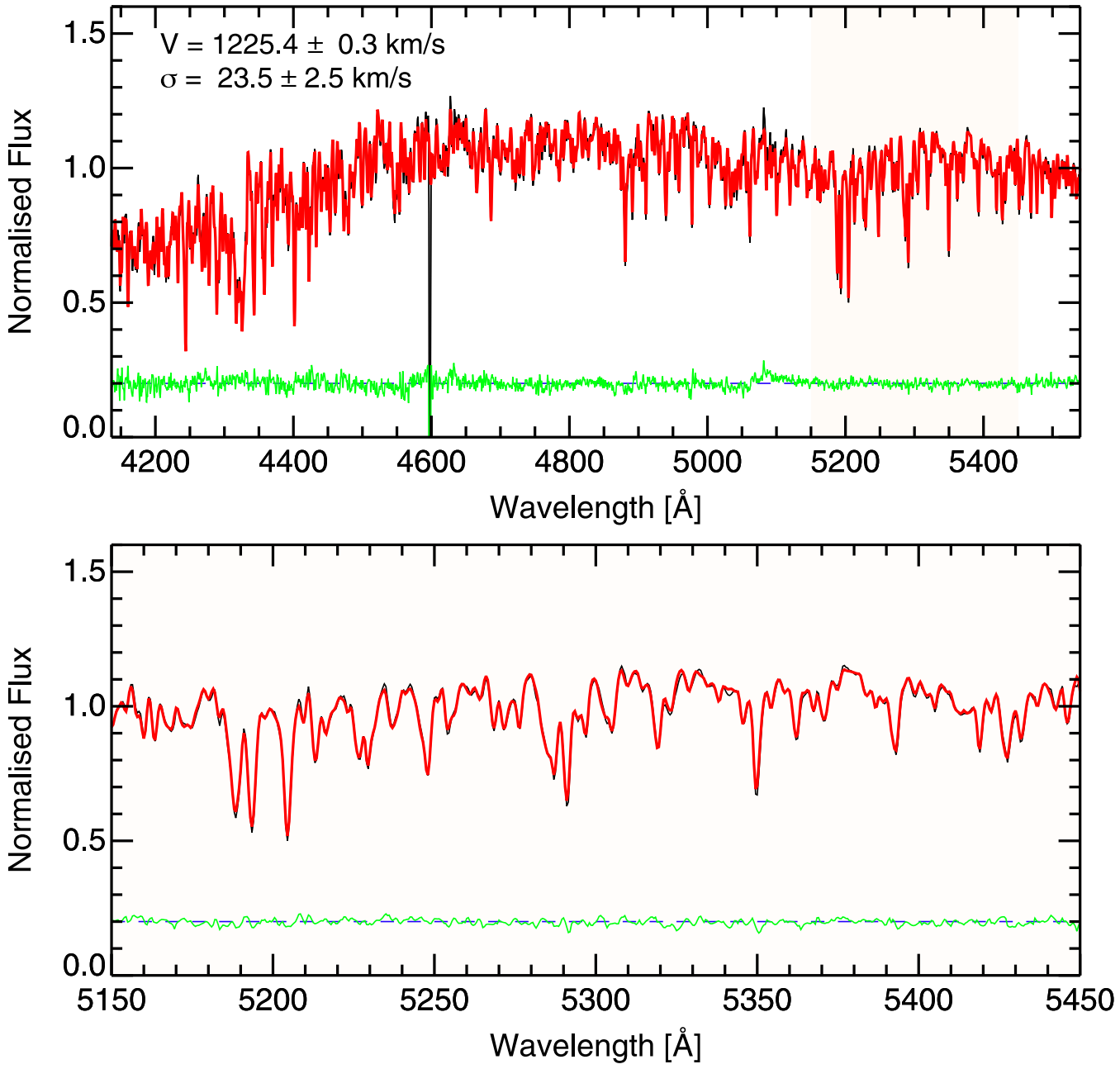

Figure 1. Upper panel: integrated spectrum of NGC 4546-UCD1. The black line is the spectrum, and the red line is the best fit found by PPXF using the models of Maraston & Strömbäck (2011). The best-fitting kinematics are provided in the upper left. The green line shows the residuals (offset by 0.2 to make them visible), and the blue dashed line behind the green line shows the no residuals line for a perfect fit. The residual features at ∼4600 and 5080 Å are due to chip gaps and are masked during the fitting. The shaded region indicates the region displayed in the lower panel. Lower panel: zoom-in of the region between 5150 and 5450 Å to demonstrate the high quality of the fit.

2010; Lyubenova et al. 2013), where again one rotating component is typically observed to be younger than the other population. Only higher spatial and spectral resolution data ideally from IFU spectroscopy will be able to confirm the significance of this feature.

It is important to note that the rotation amplitude measured is only a lower limit as the slitlet was arbitrarily aligned with the UCD and likely misses the direction of peak rotation. In fact, the position angle of this UCD, which is slightly flattened ($b/a = 0.92$), is around 82°, which means that the slitlet was almost perfectly aligned with the minor axis of the UCD, and further supports the possibility of significant rotation being present but unobservable with this data set. It is not clear what rotation amplitude, if any, a UCD should be expected to have, as only two previous measurements have been made. Typical GCs do indeed rotate with a few km s^{-1} (Bianchini et al. 2013; Kimmig et al. 2015; Lardo et al. 2015), as does UCD3 in the Fornax cluster (Frank et al. 2011), while the NSC of NGC 4244 rotates with an amplitude of ∼30 km s^{-1} (Seth et al. 2008) and the unusually dense UCD, M60-UCD1, is observed to rotate with amplitude as high as 40 km s^{-1} (Seth et al. 2014). A rotation amplitude of this magnitude would be clearly visible in our data, except that the slit may be aligned almost perfectly along the zero-velocity contour.

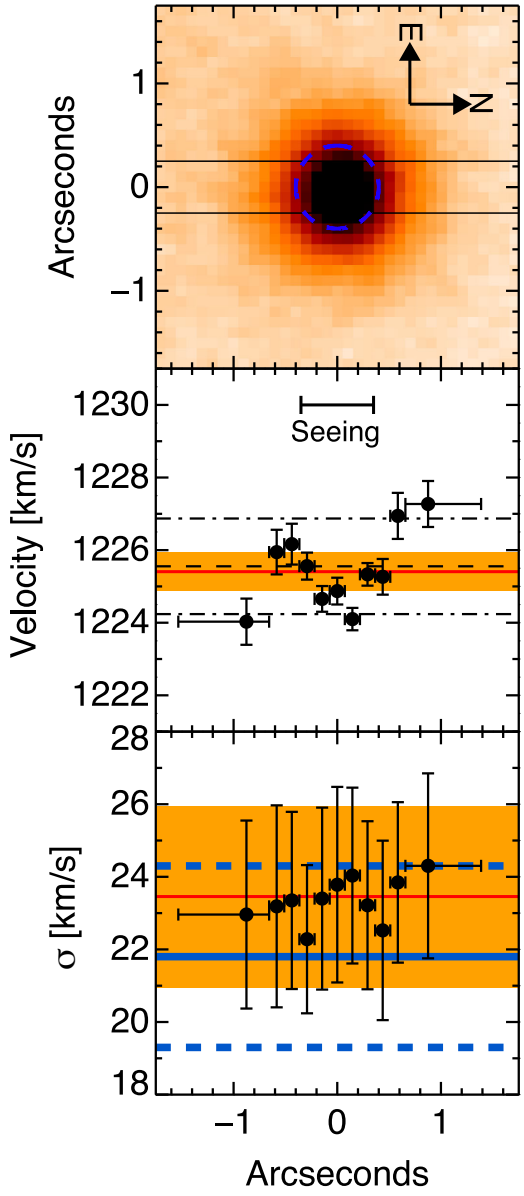

Figure 2. Upper panel: thumbnail image (3.5 arcsec × 3.5 arcsec) of NGC 4546-UCD1 from *HST* WFPC2 *F606W* imaging. The black lines indicate the size and orientation of the 0.5 arcsec slit used in this study. The blue dashed circle indicates the radius encompassing half the flux of NGC 4546-UCD1. Middle panel: the spatially resolved velocity of NGC 4546-UCD1. The *x*-axis error bars show the lower and upper limits of the binned spectra, the dot shows the light weighted centre of each bin. The red line and orange bands show the recessional velocity and its 1σ uncertainties as measured from the integrated spectrum. The dashed line shows the most probable central velocity, as fitted to the spatially resolved velocities, and the dot–dashed lines the most probable maximum and minimum velocities of the rotation curve. The most probable amplitude of rotation is 1.3 km s^{-1}. The integrated seeing of 0.7 arcsec is indicated at the top of the panel. Lower panel: the velocity dispersion profile of the UCD. The red line and orange region again show the velocity dispersion and its 1σ uncertainty as measured from the integrated spectrum. The blue solid line and the blue dashed lines show the velocity dispersion and its 1σ error measured in Norris et al. (2014a) using a spectrum from the SOAR telescope. The velocity dispersion is consistent with being flat over the full extent of the UCD.

In contrast with the rotation curve, the velocity dispersion profile of NGC 4546-UCD1 is consistent with being flat, indicating that either we lack sufficient resolution or that unlike M60-UCD1, this UCD does not host a massive black hole at its centre.

3.2 Luminosity-weighted stellar populations

In order to compare the integrated stellar population parameters of NGC 4546-UCD1 to previous lower S/N measurements for the same object, and to literature measurements of GCs, we undertake a simple Lick/IDS line strength analysis (Worthey & Ottaviani 1997; Trager et al. 1998). Due to the high S/N of our input spectrum, the statistical uncertainties on this analysis are unreasonably small. Therefore, to derive more realistic errors on the derived stellar population parameters, we attempt to determine their systematic uncertainties by using several different sets of SSP models.

First we use the method outlined in Norris et al. (2008); the Lick/IDS line strengths are measured from the flux-calibrated GMOS spectrum, and then we apply small offsets in order to bring the GMOS indices into better agreement with the Lick/IDS system (see Norris, Sharples & Kuntschner 2006; Norris et al. 2008, for more details). We then use the procedure outlined in Norris & Kannappan (2011) to convert our measured Lick/IDS indices into integrated stellar population parameters for the UCD. In short, we use the χ^2-minimization approach of Proctor, Forbes & Beasley (2004). To ensure a smooth model grid, we first interpolate the SSP models of Thomas, Maraston & Bender (2003) and Thomas, Maraston & Korn (2004) to a finer model grid, and then we perform a χ^2-minimization on the resulting age, [*Z*/H], and [α/Fe] space. Errors come from 50 Monte Carlo resimulations of the input data within the measured index errors.

Secondly, we utilize the same method outlined above except that we make use of the latest version of the Thomas, Maraston & Johansson (2011) models. In this version of the models, no offset to the Lick/IDS system is required, as the models are computed for flux-calibrated spectra such as ours. In addition, two flavours of model are provided for two sets of isochrones. We therefore fit both for both sets of isochrones. We take the resulting fits from the Padova isochrone-based models as our best-fitting SSP-equivalent stellar populations.

We then estimate the uncertainties on the derived SSP-equivalent stellar population parameters by looking at the scatter in the derived stellar populations from the three available model sets [the single Thomas et al. (2003, 2004) model set and the two Thomas et al. (2011) model sets].

Using the first procedure outlined above, with a more restrictive set of available indices measured from the SAURON spectrum of the UCD, Norris & Kannappan (2011) found age $= 3.4^{+1.7}_{-1.2}$ Gyr, [*Z*/H] $= 0.21 \pm 0.14$, and [α/Fe] $= -0.01 \pm 0.08$. Using our high-S/N, wider wavelength coverage spectrum, we find that the UCD has age $= 3.99^{+0.93}_{-0.75}$ Gyr, [*Z*/H] $= 0.18 \pm 0.06$, and [α/Fe] $= 0.05 \pm 0.05$, values entirely consistent with those derived previously.

3.3 The SFH of NGC 4546-UCD1

Because the integrated spectrum of NGC 4546-UCD1 is of such high quality (S/N of 50–200), we are also able to examine the temporally resolved SFH of the UCD. To do this, we make use of a similar approach to that outlined in McDermid et al. (2015). We again use the PPXF code used previously to derive the UCD kinematics; in this instance we make use of the regularization feature

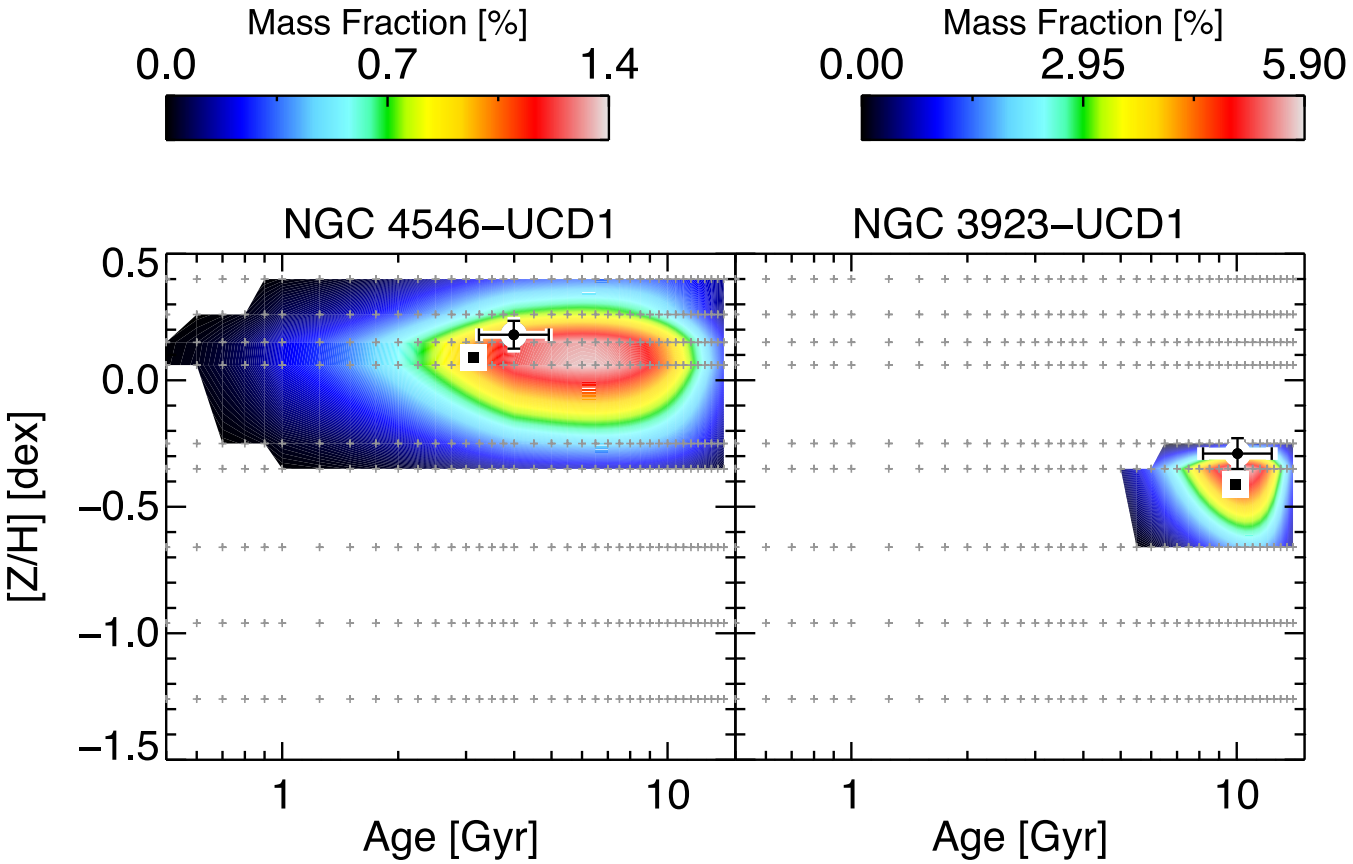

Figure 3. Left-hand panel: the SFH found by fitting the integrated spectrum of NGC 4546-UCD1, with the SSP models of Vazdekis et al. (2015) using PPXF. The coloured contours indicate the weight of each SSP model which is equivalent to the zero-age mass distribution of the SFH, and white regions indicate models which contribute no flux to the best-fitting model. The small grey plus symbols indicate the age and [*Z*/H] of each of the available models. The white circle with the black dot indicates the location of the luminosity-weighted SSP age and metallicity of this object as measured using absorption line strength indices (Section 3.2). The black and white square shows the location of the luminosity-weighted age and metallicity derived from the full spectral fitting. Right-hand panel: the SFH of the suspected massive GC-type UCD NGC 3923-UCD1. The black and white dots and squares are the same as in the left-hand panel.

to fit a linear combination of SSP models to our UCD spectra. Unfortunately, due to the very high luminosity-weighted metallicity of NGC 4546-UCD1 derived in the previous section, we are unable to use the Maraston & Strömbäck (2011) high-resolution models used in the kinematic analysis, as these only extend to [*Z*/H] = 0.3 dex and this leads to artefacts with the solutions running into the edge of the available model parameter space. Likewise we are also unable to use the MIUSCAT SSP models of Vazdekis et al. (2012), which have been successfully utilized to determine the SFHs of early-type galaxies (e.g. McDermid et al. 2015), as they similarly do not extend to sufficiently high metallicity (maximum [*Z*/H] = 0.22 dex). We therefore make use of the newest MILES-based models from Vazdekis et al. (2015). These models extend to [*Z*/H] = 0.4 dex for their BaSTI isochrone-based version, and furthermore provide a choice of IMF and alpha-enhancement ratio. For this work, we use the revised Kroupa IMF-based models (see Vazdekis et al. 2015 for full details), and assume solar-alpha enhancement in order to properly account for the measured [α/Fe] of NGC 4546-UCD1. The chosen models span a range in age of 0.03–14 Gyr, and [*Z*/H] from −2.27 to +0.4 dex, providing a total of 636 models in all. As the resolution of the MILES models is lower than our spectra (FWHM = 2.51 Å versus 1.41 Å), we are forced to smooth our input spectra in order to match the lower resolution of the templates.

The regularization prescription used by PPXF is designed to reduce the degeneracies present when fitting SFHs to the integrated spectra of complex stellar systems. It enforces the situation that adjacent models in the grid must have weights that vary smoothly, with the result that the fitted SFH is the smoothest solution that is consistent with the noise. Despite this requirement, bursty SFHs are not prevented, only that the burst will appear somewhat broadened to include adjacent models. As the SSP models used here are normalized to an initial birth mass of 1 solar mass, the distribution of PPXF weights recovers the contribution of each SSP to the zero-age mass distribution, which is equivalent to the SFH of the population.

Fig. 3 shows the resulting SFHs derived using this procedure. As well as NGC 4546-UCD1, we also fit the SFH of the suspected GC-type UCD NGC 3923-UCD1. The spectrum of NGC 3923-UCD1 was obtained with GMOS using exactly the same setup as the spectrum of NGC 4546-UCD1; it was first presented in Norris et al. (2012) and provides a perfect comparison spectrum. The analysis of the luminosity-weighted age and metallicity of NGC 3923-UCD1 (plus the additional UCDs of NGC 3923) will be presented in Janz et al. (in preparation), where the analysis follows a similar method to that taken in Section 3.2. The derived age of NGC 3923-UCD1 is $10.05^{+2.28}_{-1.87}$ Gyr, its metallicity is [*Z*/H] = −0.29 ± 0.06, and [α/Fe] = 0.24 ± 0.04, meaning this object has properties entirely consistent with a typical GC.

The white and black circles and squares in Fig. 3 display the luminosity-weighted age and metallicity of the UCDs, with the circles indicating the luminosity-weighted populations measured from the line-index-based method described above (age = 3.99 Gyr, [*Z*/H] = 0.18 dex, and age = 10.05 Gyr, [*Z*/H] = −0.29 dex for NGC 4546-UCD1 and NGC 3923-UCD1, respectively). The squares indicate the luminosity-weighted populations as derived from the full spectral fitting method (age = 3.13 Gyr, [*Z*/H] = 0.09 dex, and age = 9.91 Gyr, [*Z*/H] = −0.41 dex for NGC 4546-UCD1 and NGC 3923-UCD1, respectively). The fact that both methods provide consistent results provides additional confirmation of the reliability of the full spectral fitting approach.

From Fig. 3 it is clear that NGC 4546-UCD1 appears to have had an extremely extended SFH, with stars forming from the earliest periods up until around 1 Gyr ago (as strongly hinted at by the young luminosity-weighted age of the UCD). In order to test how robust this finding is, we have attempted to examine how many separate star formation events would be required to produce an observed SFH like this one. To do this, we created single-, dual-, and triple-burst SFHs using the same Vazdekis et al. (2015) models used to fit the data. The models had metallicity of 0.06, 0.11, or 0.15 dex (as we are attempting to reproduce the SFH shown in Fig. 3, not the integrated properties of the UCD), and to keep the problem tractable each burst was assumed to have equal weight in the final light (i.e. later bursts formed fewer stars). The resulting spectra were then degraded to have the same S/N as the spectrum of NGC 4546-UCD1 (i.e. ∼200 Å) and then were fitted with PPXF in the same manner as the real spectrum. The result of this procedure is that few models could reproduce the integrated properties of the UCD, and no single or double burst was able to reliably reproduce the SFH seen in Fig. 3, in the sense that they could not reproduce either the distribution of ages and metallicities, or the relative weights of each model observed in Fig. 3. However, a triple-burst model with bursts at 3, 6, and 10 Gyr and fixed metallicity of 0.11 dex did do a reasonable job of approximating the best-fitting SFH, and of matching the integrated properties of the UCD. We therefore conclude that the UCD has had an extended SFH, but cannot determine if this history was continuous, bursty, or a combination of both modes.

The metallicity evolution indicated by Fig. 3 is also particularly interesting, as at the earliest epoch the metallicity of the object was already high, at least near-solar values. This high initial metallicity at early times implies that this object formed in an already highly enriched medium, which in turn implies that the object was most likely located in the very centre of a fairly massive halo in the early Universe. The high absolute value of the metallicity is also unusual for most galaxy populations; only 38 out of 259 galaxies from the ATLAS^{3D} have [*Z*/H] > 0.15 within $R_e/8$. This means that this UCD is as metal rich as the inner regions of some of the most massive galaxies. Such high metallicities do however appear to be a fairly common property of suspected stripped-nucleus UCDs (Janz et al., in preparation); in particular the confirmed stripped-nucleus UCD M60-UCD1 has an almost identical total metallicity of around 0.19, although with a lower [Fe/H] of around solar (Strader et al. 2013).

The subsequent metallicity evolution of the NGC 4546-UCD1 is also intriguing. The fact that the metallicity remained fairly constant during the period of star formation indicates that either fresh gas or lower metallicity stars from outside the UCD was regularly accreted on to the proto-UCD, presumably from a gas-rich and star-forming galactic disc. The accretion of fresh gas or stars from further out in the original galaxy may also explain the observed kinematic features described in Section 3.1.2, as any accreted gas or stars would likely form dynamically distinct structures.

It is noteworthy that the SFH of NGC 4546-UCD1 is remarkably similar to those found for a sample of seven low-redshift massive compact galaxies by Ferré-Mateu et al. (2012). In particular, the high metallicity and relatively large fraction of stars formed recently in both the galaxies and NGC 4546-UCD1 are unusual in most low-redshift early-type populations, perhaps hinting at commonalities between the formation mechanism of NGC 4546-UCD1 and these higher mass objects. It is also intriguing that the implied extended SFH (but not the metallicity enrichment history) of NGC 4546-UCD1, which was extended over ∼10 Gyr, and potentially composed of a series of short bursts, looks remarkably similar to that observed for the presumed nucleus (the GC M54) and superposed core of the Sagittarius dwarf galaxy (Siegel et al. 2007). In Sagittarius, the core + M54 region has an SFH that involved several distinct bursts over at least 10 Gyr, with the last star formation possibly occurring within the last Gyr.

In contrast, the behaviour of the suspected GC-type UCD NGC 3923-UCD1 is exactly as expected for an object formed in a single burst with a fixed metallicity. The model fits are in excellent agreement with the age and metallicity derived from the Lick analysis, and the spread in age and metallicity is entirely explainable due to model degeneracies and fitting errors.

3.4 Stellar mass

We make use of two independent approaches to estimate the stellar mass of NGC 4546-UCD1.

First, as in Norris et al. (2014a), we use a modified version of the stellar mass estimation code presented in Kannappan & Gawiser (2007) and subsequently updated in Kannappan et al. (2013, first model grid described therein). This code fits photometry from the Johnson–Cousins, Sloan, and 2MASS systems with an extensive grid of models from Bruzual & Charlot (2003) assuming a Salpeter IMF, to be rescaled as will be described shortly. The input photometry (provided in Table 1) is fitted by a grid of two-SSP, composite old + young models with ages from 5 Myr to 13.5 Gyr and metallicities from $Z = 0.008$ to 0.05. The two-component nature of this fitting procedure is ideally suited for a determination of a complex stellar population such as that spectroscopically observed in NGC 4546-UCD1. This is because the two-component nature of the fitting procedure provides a reasonable approximation of an extended SFH, allowing the accurate recovery of the true integrated M/L. The stellar mass is determined by the median and 68 per cent confidence interval of the mass likelihood distribution binned over the grid of models.

We rescale the derived stellar masses by a factor of 0.7 in order to match the 'diet' Salpeter IMF of Bell & de Jong (2001). This is done both to bring the stellar mass estimates from this technique into better agreement with estimates (such as the second approach provided below) made assuming a Chabrier- or Kroupa-type IMF and because such IMFs appear to be a better fit to observational data than Salpeter for both GCs (Strader, Caldwell & Seth 2011) and relatively low mass early-type galaxies (those with $\sigma_e \sim 90\,\mathrm{km\,s^{-1}}$; Cappellari et al. 2013). Using this approach, we measure a stellar mass of $3.27^{+0.85}_{-0.90} \times 10^7\,\mathrm{M}_\odot$.

Secondly, we make use of the newly derived near-infrared M/L presented in Norris et al. (2014b) and Norris et al. (in preparation) in combination with the luminosity-weighted stellar population parameters measured in Section 3.2. This approach has the advantage

that the reduced sensitivity of the M/L to stellar population age and metallicity in the near-IR (Meidt et al. 2014; Norris et al. 2014b; Röck et al. 2015) translates directly into a reduced sensitivity to SFH (Norris et al., in preparation). In fact, as demonstrated in Norris et al. (in preparation), where luminosity-weighted (i.e. SSP-equivalent) age and metallicity are available for a composite stellar population with SSP age > 2 Gyr, the SSP-equivalent M/L is always within 10 per cent of the true integrated M/L, irrespective of the SFH. For the UCD's measured age of 3.99 Gyr and [Z/H] of 0.18 dex, the M/L models of Norris et al. (in preparation) predict an M/L of $0.53^{+0.05}_{-0.05}$ in the IRAC 3.6 μm band. We convert the measured IRAC 3.6 μm magnitude derived in Section 2.3 (14.4 mag) to total luminosity using the absolute magnitude of the Sun $M_{\odot}^{3.6\,\mu m} = 3.24$ (Oh et al. 2008) and an assumed distance modulus to NGC 4546 of 30.58 ± 0.2. This conversion leads to a total luminosity in the 3.6 μm band of $5.87^{+1.51}_{-1.51} \times 10^7$ $L_{\odot}$, where most of the uncertainty arises from the relatively poorly constrained distance to NGC 4546. This luminosity when combined with the appropriate M/L yields a stellar mass of $3.11^{+0.66}_{-0.66} \times 10^7$ $M_{\odot}$.

3.5 Dynamical modelling

In this section, we use two approaches to estimate the total dynamical mass of NGC 4546-UCD1 and also search for evidence of the existence of an SMBH within this UCD.

3.5.1 Virial mass

We first estimate the dynamical mass of NGC 4546-UCD1 using the virial equation:

$$M_{\rm vir} = \frac{C\sigma^2 R}{G}, \quad (1)$$

where C is the virial coefficient, R is a measure of the size of the system, and σ is an estimate of the system's velocity dispersion. The exact value of C varies depending on the structure of the object, but using equation 11 from Bertin, Ciotti & Del Principe (2002) we are able to convert the measured Sérsic n value for this UCD (1.4) into a virial coefficient of 7.8. Note that this value of C is larger than the fixed value of 6.5 adopted by Forbes et al. (2014) in their analysis of a sample of GCs, UCDs, and cEs including NGC 4546-UCD1. This different choice of value of C is responsible for most of the difference between our derived virial mass and theirs. We use the measured effective radius of 25.5 pc as the measure of the size of the system.

The measured velocity dispersion must then be adjusted to take into account the fact that our slit has a finite width, and that this width is of similar size to both the seeing and the half-light radius of the UCD. This means that our measured velocity dispersion is intermediate between the central (σ_0) and global (σ_∞) velocity dispersions. We therefore use the slit size (both width and length integrated over), seeing, and half-light radius and the best-fitting Sérsic index from the *HST* imaging (described in Norris & Kannappan 2011) to calculate the correction between aperture velocity dispersion and infinite velocity dispersion following the approach of Strader et al. (2011). As expected the correction factor is small, 0.92, leading to an 18 per cent decrease in the derived total mass over using the aperture velocity dispersion. The final virial mass arrived at, when applying the correction, is $M_{\rm vir} = 2.17^{+0.51}_{-0.51} \times 10^7$ $M_{\odot}$. This mass is considerably larger than the value of $M_{\rm vir} = 1.54^{+0.43}_{-0.43} \times 10^7$ $M_{\odot}$ found in Forbes et al. (2014), with the difference due principally to the use of an object-specific choice of C for this UCD.

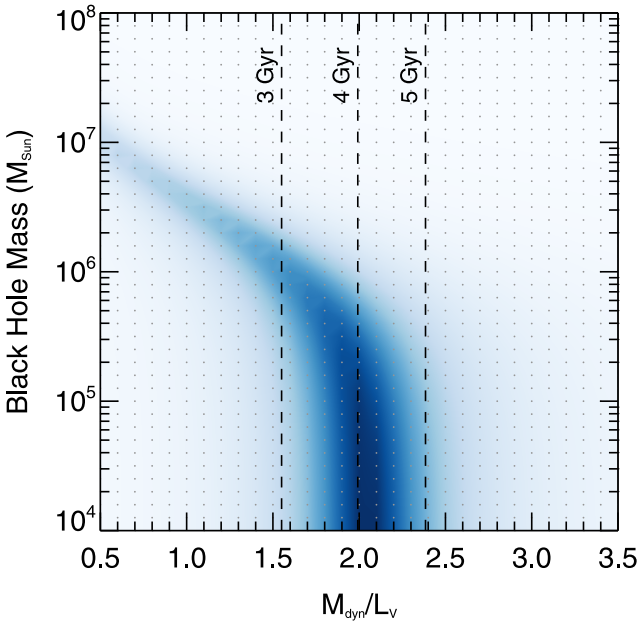

Figure 4. The goodness of fit from the JAM modelling of NGC 4546-UCD1. The shading indicates the best-fitting models; the small dots indicate the values of $M_{\rm dyn}/L_V$ and black hole mass that were fitted to the data. The dashed lines show the predicted M/L for SSP models with a Kroupa IMF, [Z/H] $= +0.35$, and 3, 4, and 5 Gyr (Maraston 1998, 2005).

3.5.2 Jeans mass modelling

Given the observed flat velocity dispersion profile, we do not expect that this UCD hosts a particularly massive black hole like the one found in M60-UCD1 (Seth et al. 2014). However, we have carried out a simple Jeans analysis both to test this suspicion and to examine the remaining tension between the dynamical and stellar masses of this UCD.

We start by using GALFIT (Peng et al. 2002) to fit a Sérsic profile to the available *HST* WFPC2 planetary camera *F606W* band imaging. This imaging had the large-scale galaxy background from NGC 4546 removed using the approach described in Norris & Kannappan (2011). The GALFIT modelling of the light distribution made use of a simulated TINYTIM (Krist 1995) point spread function constructed at the location of the UCD, as no suitable stars were located within the PC chip field of view. The resulting fit was excellent, yielding a half-light radius consistent with the one derived from a curve-of-growth analysis, a Sérsic n of 1.4, and an ellipticity very close to 1 (0.92).

These values, along with the total integrated V-band magnitude of the UCD, were then used to produce a multi-Gaussian expansion (MGE) model of the UCD light distribution as a required input for a Jeans Anisotropic MGE (JAM; Cappellari 2008) dynamical model of the UCD. We use the IDL implementation of the JAM code[3] and fit a series of simple spherical Jeans models to our measured resolved kinematics and the MGE model of the light distribution. We fit models with $M_{\rm dyn}/L_V$ varying from 0.5 to 3.5, and black hole mass from 10^4 to 10^8 $M_{\odot}$.

Fig. 4 shows the result of this fitting procedure. As expected, we are only able to place an upper limit on the black hole mass; the black hole can have any mass less than around 10^6 $M_{\odot}$, without being in significant tension with the stellar M/L expected for the UCD's age

[3] Available at http://www-astro.physics.ox.ac.uk/mxc/software/

and metallicity. Furthermore, the best-fitting dynamical M/L (of 2) is indistinguishable from a purely stellar M/L for a stellar population with the same parameters as NGC 4546-UCD1, indicating that there is little sign of a significant dark mass component within this UCD, be it a black hole or dark matter. The result of the fitting does however provide additional confirmation that the dynamical mass of the UCD is consistent with the stellar mass of the UCD only when the UCD is relatively young.

It is worth noting that assuming that the UCD mass is the same as the original central NSC, a black hole of sufficient mass to be detectable is not necessarily expected. Using the relation between central massive object (either NSC or SMBH) and total dynamical galaxy mass from Ferrarese et al. (2006) implies that the original host galaxy of the UCD should have had a dynamical mass of 1–2 $\times$ 10^{10} $M_\odot$ (and therefore a total stellar mass of several $\times 10^9$ $M_\odot$). This mass is similar to that of M33 (Corbelli 2003), the Local Group spiral galaxy which also hosts an NSC with very similar velocity dispersion to that of NGC 4546-UCD1 ($\sigma_e = 24 \pm 1.2$ km s^{-1}), but has no detectable black hole down to an upper limit of 1500 $M_\odot$ (Gebhardt et al. 2001). Similarly, the NSC of NGC 404 which has a similar dynamical mass as NGC 4546-UCD1 (1.1×10^7 $M_\odot$) also lacks a black hole more massive than 5×10^5 $M_\odot$ (Seth et al. 2010). In fact, apart from M60-UCD1 no object with a mass $< 10^{10}$ $M_\odot$ is known to host a black hole more massive than 10^6 $M_\odot$ (Miller et al. 2015).

The fact that we find the most likely black hole masses to be consistent with those of SMBHs found in galaxies similar to the expected progenitor galaxy implies that while the progenitor galaxy was destroyed the central bound structure that was left to evolve into NGC 4546-UCD1 cannot itself have been heavily stripped. If the opposite was true, and the UCD itself was significantly stripped, we would likely find a black hole significantly overmassive relative to the expected mass, as is the case for M60-UCD1. This apparently low black hole mass also supports the idea that the progenitor of NGC 4546-UCD1 was a small dwarf galaxy with an NSC, not a genuine bulge. This is in contrast to the situation for M60-UCD1, where the black hole is clearly detected and has a mass of 2.1×10^7 $M_\odot$ within a UCD of only 1.2×10^8 $M_\odot$. Using the same scaling relations implies that original central bound structure mass of M60-UCD1 was around 100 times larger than is left in the UCD, and at a mass of $\sim 10^{10}$ $M_\odot$ this structure was clearly a genuine bulge. Further evidence for this picture is provided by the observed two-component structure of M60-UCD1, with one of the structures having properties consistent with being an NSC embedded within the remnants of the mostly stripped bulge (Seth et al. 2014).

Under the assumption that NGC4546-UCD1 either never contained any dark matter or has been so thoroughly stripped that it has lost any significant dark matter component within the region our measured dynamics probe, we can also make an estimate of the total dynamical mass using the best-fitting $M_{\rm dyn}/L_V$. This is because under these assumptions $M_{\rm dyn}/L_V = M_\star/L_V$. The best-fitting $M_{\rm dyn}/L_V$ was 2.0, which when using the total V-band magnitude of the UCD listed in Table 1 translates into a total dynamical mass of $M_{\rm dyn} = 2.59^{+0.49}_{-0.49} \times 10^7$ $M_\odot$.

The two estimates of dynamical mass are in good agreement, and furthermore are in reasonable agreement with the stellar masses derived in Section 3.4. In fact, when considering their mutual errors the dynamical mass-to-stellar mass ratio of NGC 4546-UCD1 is now consistent with being 1. A similar finding of consistent dynamical and stellar mass estimates was also found for a sample of nine NSCs by Walcher et al. (2006), where the M/L derived from dynamics and from stellar populations were found to be consistent with 1. This is further proof that the dynamics of this UCD (and even NSCs) can be explained without the need to invoke exotic IMFs or the presence of dark matter or massive dark objects like black holes.

4 NGC 4546-UCD1'S GALACTIC ORIGIN

We have examined the spatially resolved kinematics and SFH of NGC 4546-UCD1, a UCD suspected of being the result of a tidal interaction between NGC 4546 and a dwarf companion of mass around 3 $\times$ 10^9 $M_\odot$ [Norris & Kannappan 2011, based on the observed relation between the nuclear mass of a galaxy and its spheroid from Graham & Spitler (2009)].

Our observation that NGC 4546-UCD1 has disordered kinematics is readily understandable in such a scenario, as NSCs are often observed to have such complex kinematic structures (Seth et al. 2010; Lyubenova et al. 2013). In this context, these structures are thought to result from either the accretion of fresh gas and subsequent star formation *in situ* in the NSC (as seen for example in the Milky Way NSC; Bartko et al. 2010; Pfuhl et al. 2011) or alternatively from the accretion of entire star clusters formed externally which have inspiralled into the NSC from larger radii due to tidal friction (see e.g. Antonini et al. 2012; Antonini 2013).

A more conclusive indicator of the galactic origin of NGC 4546-UCD1 is provided by the temporally extended SFH of this UCD. The very extended nature of the star formation, which appears to have extended from the earliest epochs until a few Gyr ago, conclusively rules out a star cluster origin for this object. This interpretation is further confirmed by the SFH of the suspected GC-type UCD which is entirely consistent with NGC 3923-UCD1 forming in a single-metallicity burst $\sim$10 Gyr ago, indicating the soundness of our derived SFHs.

The fact that there does not appear to be significant metallicity evolution during the period where NGC 4546-UCD1 was forming stars indicates that the proto-UCD was constantly accreting fresh gas (as expected if the star formation was to continue for such an extended period). This observation fits naturally with a picture where an NSC accretes fresh lower metallicity gas from the galaxy's disc, or alternatively accretes star clusters which have inspiralled from the disc. The high absolute value of the metallicity also supports an origin of this object as the central region of a relatively massive galaxy, as only massive galaxies are able to enrich to such extreme metallicities. The fact that our inferred galaxy mass is lower than that expected for a galaxy with such high metallicity perhaps indicates an emerging tension with the very high metallicities observed in known stripped-nucleus UCDs (i.e. M60-UCD1 also has [Z/H] $\sim$ +0.2). Examination of a larger sample of confirmed stripped nuclei will be required to address this tension further.

We can now sketch out a complete picture of the history of NGC 4546-UCD1 that starts with it forming in the core of a dwarf galaxy at early epochs. For the next 10+ Gyr, it continued to form stars at a low rate, with occasional acquisition of lower metallicity gas or already formed stars (in the form of inspiralling star clusters) from the galaxy's disc. Then some point in the last 1–3 Gyr it began a final interaction with NGC 4546 which led to the destruction of the main body of the dwarf galaxy, and hence cut the nucleus off from a supply of fresh gas or stars. The exact timing of the interaction is difficult to judge as the errors on the youngest age component are not inconsiderable, and there is also the possibility that star formation continued for some period after the stripping event, using up gas already present in the nuclear regions (it is also possible that the interaction funnelled more gas to the nucleus). One way to more

precisely date the interaction would be if some bona fide GCs were formed from material from the dwarf during the merger event, and now survive mixed in amongst the previously existing GCs of NGC 4546.

5 CONCLUSIONS

We have used deep spectroscopic observations of NGC 4546-UCD1, one of the closest UCDs to examine its stellar populations and SFH. We find evidence that the internal kinematics of this object are complex, and possibly indicative of multiple periods of star formation. This suggestion is confirmed by our analysis of the SFH of this object, which confirms that NGC 4546-UCD1 was forming stars from the earliest epochs until 1–2 Gyr ago. Such an SFH is not expected in a star cluster and can only be found in true galactic populations, thereby confirming that this UCD is the remnant nucleus of a galaxy tidally disrupted by NGC 4546. Comparison with the SFH of another UCD, NGC 3923-UCD1, that is suspected of being a massive star cluster demonstrates that the extended SFH of NGC 4546-UCD1 is a robust detection, and further supports the contention that UCDs are a composite population of massive star clusters and stripped galaxy nuclei.

We suggest that similar spectroscopic observations of other UCDs may provide a more observationally straightforward method (compared to AO-assisted kinematic studies) to detect objects formed by tidal interactions.

ACKNOWLEDGEMENTS

The authors would like to thank the referee, whose very constructive comments significantly improved this work. In addition, they would also like to thank Alexandre Vazdekis for providing the latest version of his stellar population synthesis models prior to public release. They would like to thank Glenn van de Ven and Eva Schinnerer for their very helpful discussions which greatly improved this manuscript, and Jay Strader for computing the correction factors used to correct measured aperture velocity dispersion to total velocity dispersion. CGE and FRF acknowledge financial support from Consejo Nacional de Investigaciones Científicas y Técnicas (PIP 0393), and Universidad Nacional de La Plata, Argentina (G128).

This work is based on observations obtained at the Gemini Observatory, as part of programmes GS-2011A-Q-13, GS-2013A-Q-26, GS-2014A-Q-30, and processed using the Gemini IRAF package. The Gemini Observatory is operated by the Association of Universities for Research in Astronomy, Inc., under a cooperative agreement with the NSF on behalf of the Gemini partnership: the National Science Foundation (United States), the National Research Council (Canada), CONICYT (Chile), the Australian Research Council (Australia), Ministério da Ciência, Tecnologia e Inovação (Brazil) and Ministerio de Ciencia, Tecnología e Innovación Productiva (Argentina).

Support for programme number HST-AR-12147.01-A was provided by NASA through a grant from the Space Telescope Science Institute, which is operated by the Association of Universities for Research in Astronomy, Inc., under NASA contract NAS5-26555.

This work is also based in part on observations made with the *Spitzer Space Telescope*, which is operated by the Jet Propulsion Laboratory, California Institute of Technology under a contract with NASA.

This research has made use of the NASA/IPAC Extragalactic Database (NED) which is operated by the Jet Propulsion Laboratory, California Institute of Technology, under contract with the National Aeronautics and Space Administration.

REFERENCES

Antonini F., 2013, ApJ, 763, 62
Antonini F., Capuzzo-Dolcetta R., Mastrobuono-Battisti A., Merritt D., 2012, ApJ, 750, 111
Bartko H. et al., 2010, ApJ, 708, 834
Bekki K., Couch W. J., 2003, ApJ, 596, L13
Bell E. F., de Jong R. S., 2001, ApJ, 550, 212
Bertin E., Arnouts S., 1996, A&AS, 117, 393
Bertin G., Ciotti L., Del Principe M., 2002, A&A, 386, 149
Bianchini P., Varri A. L., Bertin G., Zocchi A., 2013, ApJ, 772, 67
Brodie J. P., Romanowsky A. J., Strader J., Forbes D. A., 2011, AJ, 142, 199
Brüns R. C., Kroupa P., 2012, A&A, 547, A65
Bruzual G., Charlot S., 2003, MNRAS, 344, 1000
Cappellari M., 2008, MNRAS, 390, 71
Cappellari M., Emsellem E., 2004, PASP, 116, 138
Cappellari M. et al., 2013, MNRAS, 432, 1862
Chiboucas K. et al., 2011, ApJ, 737, 86
Corbelli E., 2003, MNRAS, 342, 199
Da Rocha C., Mieske S., Georgiev I. Y., Hilker M., Ziegler B. L., Mendes de Oliveira C., 2011, A&A, 525, A86
Decarli R., Gavazzi G., Arosio I., Cortese L., Boselli A., Bonfanti C., Colpi M., 2007, MNRAS, 381, 136
Drinkwater M. J., Jones J. B., Gregg M. D., Phillipps S., 2000, Publ. Astron. Soc. Aust., 17, 227
Drinkwater M. J., Gregg M. D., Hilker M., Bekki K., Couch W. J., Ferguson H. C., Jones J. B., Phillipps S., 2003, Nature, 423, 519
Emsellem E. et al., 2007, MNRAS, 379, 401
Faifer F. R. et al., 2011, MNRAS, 416, 155
Fellhauer M., Kroupa P., 2002, MNRAS, 330, 642
Fellhauer M., Kroupa P., 2005, MNRAS, 359, 223
Ferrarese L. et al., 2006, ApJ, 644, L21
Ferré-Mateu A., Vazdekis A., Trujillo I., Sánchez-Blázquez P., Ricciardelli E., de la Rosa I. G., 2012, MNRAS, 423, 632
Forbes D. A., Norris M. A., Strader J., Romanowsky A. J., Pota V., Kannappan S. J., Brodie J. P., Huxor A., 2014, MNRAS, 444, 2993
Frank M. J., Hilker M., Mieske S., Baumgardt H., Grebel E. K., Infante L., 2011, MNRAS, 414, L70
Fukugita M., Ichikawa T., Gunn J. E., Doi M., Shimasaku K., Schneider D. P., 1996, AJ, 111, 1748
Gebhardt K. et al., 2001, AJ, 122, 2469
Georgiev I. Y., Böker T., 2014, MNRAS, 441, 3570
Graham A. W., Spitler L. R., 2009, MNRAS, 397, 2148
Gratton R. G., Carretta E., Bragaglia A., 2012, A&AR, 20, 50
Hilker M., 2006, preprint (arXiv:e-prints)
Hilker M., Infante L., Vieira G., Kissler-Patig M., Richtler T., 1999, A&AS, 134, 75
Hook I. M., Jørgensen I., Allington-Smith J. R., Davies R. L., Metcalfe N., Murowinski R. G., Crampton D., 2004, PASP, 116, 425
Janz J., Forbes D. A., Norris M. A., Strader J., Penny S. J., Fagioli M., Romanowsky A. J., 2015, MNRAS, 449, 1716
Kannappan S. J., Gawiser E., 2007, ApJ, 657, L5
Kannappan S. J. et al., 2013, ApJ, 777, 42
Kimmig B., Seth A., Ivans I. I., Strader J., Caldwell N., Anderton T., Gregersen D., 2015, AJ, 149, 53
Krist J., 1995, in Shaw R. A., Payne H. E., Hayes J. J. E., eds, ASP Conf. Ser. Vol. 77, Astronomical Data Analysis Software and Systems IV. Astron. Soc. Pac., San Francisco, p. 349
Lardo C. et al., 2015, A&A, 573, A115
Lyubenova M. et al., 2013, MNRAS, 431, 3364
McDermid R. M. et al., 2015, MNRAS, 448, 3484
McGaugh S. S., Schombert J. M., 2015, ApJ, 802, 18
Maraston C., 1998, MNRAS, 300, 872

Maraston C., 2005, MNRAS, 362, 799
Maraston C., Strömbäck G., 2011, MNRAS, 418, 2785
Meidt S. E. et al., 2014, ApJ, 788, 144
Mieske S., Hilker M., Misgeld I., 2012, A&A, 537, A3
Miller B. P., Gallo E., Greene J. E., Kelly B. C., Treu T., Woo J.-H., Baldassare V., 2015, ApJ, 799, 98
Norris M. A., Kannappan S. J., 2011, MNRAS, 414, 739
Norris M. A., Sharples R. M., Kuntschner H., 2006, MNRAS, 367, 815
Norris M. A. et al., 2008, MNRAS, 385, 40
Norris M. A. et al., 2012, MNRAS, 421, 1485
Norris M. A. et al., 2014a, MNRAS, 443, 1151
Norris M. A., Meidt S., Van de Ven G., Schinnerer E., Groves B., Querejeta M., 2014b, ApJ, 797, 55
Oh S.-H., de Blok W. J. G., Walter F., Brinks E., Kennicutt R. C., Jr, 2008, AJ, 136, 2761
Peng C. Y., Ho L. C., Impey C. D., Rix H.-W., 2002, AJ, 124, 266
Pfeffer J., Baumgardt H., 2013, MNRAS, 433, 1997
Pfeffer J., Griffen B. F., Baumgardt H., Hilker M., 2014, MNRAS, 444, 3670
Pfuhl O. et al., 2011, ApJ, 741, 108
Phillipps S., Drinkwater M. J., Gregg M. D., Jones J. B., 2001, ApJ, 560, 201
Proctor R. N., Forbes D. A., Beasley M. A., 2004, MNRAS, 355, 1327
Querejeta M. et al., 2014, preprint (arXiv:e-prints)
Reach W. T. et al., 2005, PASP, 117, 978
Röck B., Vazdekis A., Peletier R. F., Knapen J. H., Falcón-Barroso J., 2015, MNRAS, 449, 2853
Rossa J., van der Marel R. P., Böker T., Gerssen J., Ho L. C., Rix H.-W., Shields J. C., Walcher C.-J., 2006, AJ, 132, 1074
Schlafly E. F., Finkbeiner D. P., 2011, ApJ, 737, 103
Seth A. C., Dalcanton J. J., Hodge P. W., Debattista V. P., 2006, AJ, 132, 2539
Seth A. C., Blum R. D., Bastian N., Caldwell N., Debattista V. P., 2008, ApJ, 687, 997
Seth A. C. et al., 2010, ApJ, 714, 713
Seth A. C. et al., 2014, Nature, 513, 398
Siegel M. H. et al., 2007, ApJ, 667, L57
Strader J., Caldwell N., Seth A. C., 2011, AJ, 142, 8
Strader J. et al., 2013, ApJ, 775, L6
Thomas D., Maraston C., Bender R., 2003, MNRAS, 339, 897
Thomas D., Maraston C., Korn A., 2004, MNRAS, 351, L19
Thomas D., Maraston C., Johansson J., 2011, MNRAS, 412, 2183
Toloba E. et al., 2014, ApJ, 783, 120
Trager S. C., Worthey G., Faber S. M., Burstein D., Gonzalez J. J., 1998, ApJS, 116, 1
Valluri M., Ferrarese L., Merritt D., Joseph C. L., 2005, ApJ, 628, 137
Vazdekis A., Ricciardelli E., Cenarro A. J., Rivero-González J. G., Díaz-García L. A., Falcón-Barroso J., 2012, MNRAS, 424, 157
Vazdekis A. et al., 2015, MNRAS, 449, 1177
Walcher C. J., Böker T., Charlot S., Ho L. C., Rix H.-W., Rossa J., Shields J. C., van der Marel R. P., 2006, ApJ, 649, 692
Worthey G., Ottaviani D. L., 1997, ApJS, 111, 377

This paper has been typeset from a TEX/LATEX file prepared by the author.